Molecular Therapy
Nucleic Acids
Original Article

EpCAM-Targeted 3WJ RNA Nanoparticle Harboring Delta-5-Desaturase siRNA Inhibited Lung Tumor Formation via DGLA Peroxidation

Lizhi Pang,[1] Harshit Shah,[1] Hongzhi Wang,[2,3,4] Dan Shu,[2,3,4] Steven Y. Qian,[1] and Venkatachalem Sathish[1]

[1]Department of Pharmaceutical Sciences, North Dakota State University, Fargo, ND 58102, USA; [2]Center for RNA Nanobiotechnology and Nanomedicine, The Ohio State University, Columbus, OH 43210, USA; [3]College of Pharmacy, Division of Pharmaceutics and Pharmaceutical Chemistry, The Ohio State University, Columbus, OH 43210, USA; [4]College of Medicine, Dorothy M. Davis Heart and Lung Research Institute and James Comprehensive Cancer Center, The Ohio State University, Columbus, OH 43210, USA

Knocking down delta-5-desaturase (D5D) expression by D5D small interfering RNA (siRNA) has been reported that could redirect the cyclooxygenase-2 (COX-2)-catalyzed dihomo-γ-linolenic acid (DGLA) peroxidation from producing prostaglandin E2 to 8-hydroxyoctanoic acid (8-HOA), resulting in the inhibition of colon and pancreatic cancers. However, the effect of D5D siRNA on lung cancer is still unknown. In this study, by incorporating epithelial cell adhesion molecule (EpCAM) aptamer and validated D5D siRNA into the innovative three-way junction (3WJ) RNA nanoparticle, target-specific accumulation and D5D knockdown were achieved in the lung cancer cell and mouse models. By promoting the 8-HOA formation from the COX-2-catalyzed DGLA peroxidation, the 3WJ-EpCAM-D5D siRNA nanoparticle inhibited lung cancer growth *in vivo* and *in vitro*. As a potential histone deacetylases inhibitor, 8-HOA subsequently inhibited cancer proliferation and induced apoptosis via suppressing YAP1/TAZ nuclear translocation and expression. Therefore, this 3WJ-RNA nanoparticle could improve the targeting and effectiveness of D5D siRNA in lung cancer therapy.

INTRODUCTION

As the most common type of lung cancer, non-small cell lung cancer (NSCLC) has the highest fatality rate worldwide.[1] Due to the universally high cyclooxygenase-2 (COX-2) expression in ~80% of NSCLC patients, the traditional anti-cancer concept of the COX-2 inhibitor was designed to limit the COX-2-catalyzed arachidonic acid (AA) peroxidation and the formation of its downstream molecule prostaglandin E2 (PGE2; cancer inducer) in lung cancer.[2,3] However, many COX-2 inhibitors have failed to show efficacy clinically.[4,5] Instead of inhibiting COX-2, our previous studies have demonstrated that the genetic knockdown of the delta-5-desaturase (D5D) provided a unique strategy that not only limited AA formation from dihomo-γ-linolenic acid (DGLA; ω-6 unsaturated fatty acid), but also promoted the COX-2-catalyzed DGLA peroxidation to form 8-hydroxyoctanoic acid (8-HOA).[6,7] The previous studies indicated that 8-HOA could be served as an anti-cancer free radical byproduct in colon and pancreatic cancers.[8,9] However, the effect of D5D knockdown on lung cancer is still unknown.

Despite its distinct promise *in vitro*, the clinical application of D5D knockdown via small interfering RNA (siRNA) was hindered by its instability, low bioavailability, and poor targeting to tumors.[10] Encapsulation of siRNA in the nanoparticle is a promising way to improve the effectiveness of siRNA for cancer treatment. However, the application of nanoparticle-encapsulated siRNA is confined by the low targeting efficiency, chemical and thermodynamic instability, and poor biocompatibility.[11,12] To address these issues, we have previously proposed the innovative three-way junction (3WJ) RNA nanoparticle to deliver miRNA/siRNA for cancer therapy.[13–15] The thermodynamically stable 3WJ motif derived from the phi29 packaging RNA (pRNA) core is composed of three oligos with a branched structure. The 3WJ scaffold facilitates the conjugation of diverse functional modules on each branch to form a multi-functional 3WJ RNA nanoparticle. In particular, siRNA can be easily incorporated into the branch of the pRNA-3WJ motifs via bottom-up self-assembly, which could be processed by dicer intracellularly. The 3WJ RNA nanoparticle has displayed excellent chemical stability (resistant to denaturation via 8 M urea), enzymatic stability (remain intact at 20% [v/v] FBS for up to 24 h), thermodynamic stability (unable to be dissociated at ultra-low concentrations), and favorable pharmacological profiles of biodistribution.[16–18]

In this study, 3WJ RNA nanoparticle harboring D5D siRNA and epithelial cell adhesion molecule (EpCAM) aptamer was constructed as previously described.[15] Because EpCAM has moderate to high expression in more than 70% of NSCLC patients,[19] the EpCAM aptamer could function as the targeting module to direct the

Received 16 June 2020; accepted 20 August 2020;
https://doi.org/10.1016/j.omtn.2020.08.024.

Correspondence: Venkatachalem Sathish, Department of Pharmaceutical Sciences, North Dakota State University, Sudro 203, 1401 Albrecht Blvd., Fargo, ND 58102, USA.
E-mail: s.venkatachalem@ndsu.edu

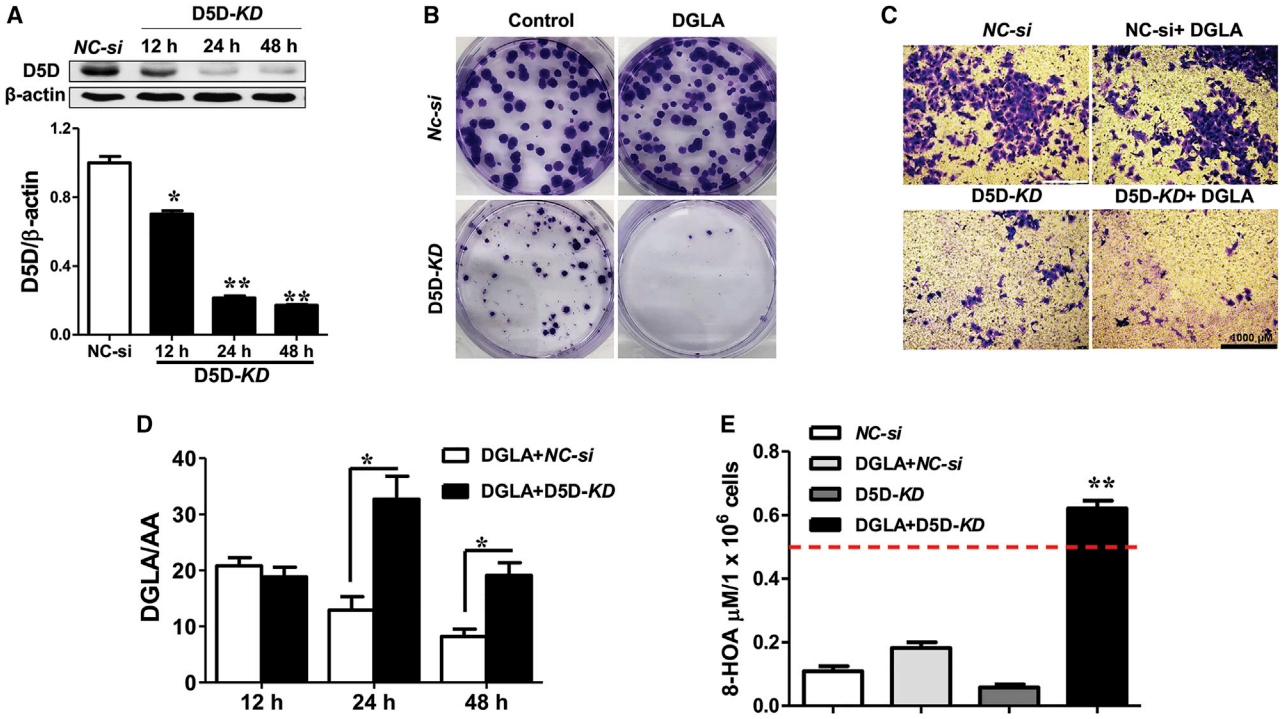

Figure 1. Delta-5 Desaturase-siRNA Knockdown Promoted Dihomo-γ-linolenic Acid's Anti-cancer Effect in A549 Lung Cancer Cells

(A) The efficiency of D5D siRNA transfection in A549 cells was shown as D5D protein expression at 12, 24, and 48 h of post-transfection by western analysis. Cells transfected with negative control siRNA (*NC-si* group) served as control. The relative expression of D5D to β-actin in the *NC-si* group was normalized to 1. (B) Colony formation of A549 cells treated with DGLA (100 μM for 48 h) and transfection of D5D siRNA or *NC-si*. Colonies were stained with crystal violet. (C) Transwell migration assay of D5D siRNA or *NC-si*-transfected A549 cells with DGLA (100 μM for 48 h) supplementation. Scale bars, 1000 μm. (D) DGLA/arachidonic acid (AA) ratio of siRNA and DGLA-treated (100 μM for 48 h) A549 cells. The DGLA and AA concentrations were measured by LC/MS after 12, 24, and 48 h of treatment. (E) 8-Hydroxyoctanoic acid (8-HOA) concentration in cell medium containing 1.0×10^6 D5D siRNA or *NC-si*-transfected A549 cells after 100 μM DGLA treatment for 48 h was determined by GC/MS quantification. The quantitative data of (B) and (C) were shown in Figures S1A and S1B, respectively. Data represent mean ± SEM for n = 3–6. $^{**}p < 0.01$, $^{*}p < 0.05$ versus *NC-si* group.

3WJ-EpCAM-D5D siRNA nanoparticle to the lung tumor. To verify the efficacy of D5D siRNA knockdown on lung cancer, we evaluated the D5D expression, cell survival, proliferation, migration, 8-HOA profile, and DGLA/AA ratio in A549 NSCLC cells. Furthermore, the 3WJ-D5D siRNA complex was synthesized for the *in vivo* distribution study. To explore the underlying mechanism of our unique treatment strategy, we also investigated the role of the histone deacetylase (HDAC)-mediated Yes-Associated protein-1 (YAP1) and transcriptional coactivator with PDZ-binding motif (TAZ) pathway in lung cancer treated with 3WJ-EpCAM-D5D siRNA nanoparticle.

RESULTS

D5D Knockdown Promoted DGLA's Anti-cancer Effect in Lung Cancer Cells

To validate the efficiency of D5D siRNA on A549 cells, we assessed the D5D protein expression in NSCLC cells using western analysis. The D5D protein band shown in Figure 1A indicated that D5D siRNA led to the most efficient knockdown of D5D protein expression in A549 cells at 48 h post-transfection (Figure 1A; $p < 0.05$). To further investigate the effectiveness of D5D siRNA on lung cancer cells, we evaluated cell proliferation and migration by using the colony formation, wound healing, and transwell assay on A549 cells. From colony formation assay, the combination of DGLA and D5D siRNA treatment group has significantly lower survival fraction (Figures 1B and S1A; $p < 0.05$), indicating that DGLA can suppress the proliferation and survival under D5D knockdown condition. From the wound healing assay shown in Figure S1D, the wound healed significantly slower in the D5D siRNA- and DGLA-treated A549 cells, suggesting the inhibition of cell migration ($p < 0.05$). Additionally, the transwell assay showed that the relative migration rate of A549 cells was significantly decreased in the DGLA + D5D siRNA treatment group (Figures 1C and S1B; $p < 0.001$). DGLA and other ω-6 fatty acids were commonly considered as the risk factor in cancer and inflammation because of AA production.[4,5,20] However, the above-mentioned assays indicated that DGLA could inhibit the A549 cell growth when concurrently knocking down the D5D protein expression in lung cancer cells. To elucidate the role of D5D on DGLA metabolism, we determined the DGLA and AA concentration in D5D siRNA-transfected A549 cells by liquid chromatography-mass spectrometry (LC/MS). The DGLA/AA ratio shown in Figure 1D indicated that D5D siRNA transfection could inhibit the AA generation from COX-2-catalyzed DGLA peroxidation. Therefore, DGLA may

start to produce other free radical byproducts, such as 8-HOA, from DGLA. To quantify the production of the 8-HOA, we used the gas chromatography-mass spectrometry (GC/MS) analysis. The formation of 8-HOA was significantly increased in D5D siRNA-transfected A549 cells (Figure 1E; $p < 0.01$), indicating that the DGLA was more likely to be peroxided to 8-HOA rather than AA by COX-2 in the D5D siRNA-transfected A549 cells. The *in vitro* efficiency of D5D siRNA was also evident by the higher 8-HOA concentration in D5D siRNA-transfected A549 cells.

3WJ-EpCAM-D5D siRNA Nanoparticles Suppressed Lung Cancer *In Vitro*

Despite the promising effect of D5D siRNA on A549 cells, it is still challenging to directly administer D5D siRNA *in vivo* due to low delivery efficacy, for example, less than 10 siRNA molecules of every 100,000 molecular injections have successfully entered cells.[21] To improve the *in vivo* efficiency of D5D siRNA in this study, we synthesized a D5D siRNA-conjugated 3WJ RNA nanoparticle (for the schematic structure, see Figure 2A) for lung cancer therapy. To validate the targeting efficiency of EpCAM-targeted 3WJ RNA nanoparticle on lung cancer, we performed the *in vitro* cell binding and internalization study on A549 cells (EpCAM positive) by using 3WJ-EpCAM-Alexa 647 nanoparticle (for tracking). The near-infrared (NIR) dye Alexa 647 was conjugated to 3′ end of the 3WJc strand as a nanoparticle tracker. The overlap between the control A549 cell population and the 3WJ-EpCAM-Alexa 647 nanoparticle-treated A549 cell population was less than 10%, suggesting that more than 90% of A549 cells can be specifically recognized by the 3WJ-EpCAM-Alexa 647 nanoparticle (shown in red peak, Figure 2B). Additionally, the cellular uptake efficiency of the nanoparticle was also confirmed by the confocal microscopy in Airyscan 2 mode. 3WJ-EpCAM-Alexa 647 nanoparticles were able to enter the cytoplasm of A549 cells within 4 h of incubation (Figure 2C). To assess the utility of EpCAM aptamer, we also measured the EpCAM expression in A549, H1299 (NSCLC), and BEAS-2B (normal lung epithelial) cells by western analysis. The EpCAM expression was significantly higher in A549 and H1299 lung cancer cells than the expression in BEAS-2B normal lung epithelial lung cells (Figure S4A; $p < 0.001$). The higher expression of EpCAM may correlate to the high affinity and internalization ability of 3WJ-EpCAM RNA nanoparticle to A549 cells.

To optimize the dose of 3WJ-EpCAM-D5D siRNA nanoparticle (without the imaging module) for lung cancer *in vitro*, we conducted thiazolyl blue tetrazolium bromide (MTT) assay on A549 cells in gradient nanoparticle concentrations for 48-h incubation along with DGLA. Among all the dose combinations, 100 μM DGLA + 100 or 1,000 nM 3WJ-EpCAM-D5D siRNA nanoparticle resulted in the lowest cell viability (Figure S1C). Therefore, 100 nM 3WJ-EpCAM-D5D siRNA nanoparticle was selected to assess the *in vitro* effect of the nanoparticle on A549 cells. To validate the knockdown efficiency of 3WJ-EpCAM-D5D siRNA nanoparticle, we performed the western analysis to assess the D5D protein level in A549 cells. The D5D expression was significantly suppressed in the 3WJ-EpCAM-D5D siRNA nanoparticle treatment group compared with the A549 cells treated with the 3WJ-EpCAM nanoparticle (Figures 2D and 2E, $p < 0.05$). By treatment of 3WJ-EpCAM-D5D siRNA nanoparticle with DGLA, the 8-HOA yield was significantly increased in the A549 cells (Figure 2F, $p < 0.01$). To evaluate the effect of 3WJ-EpCAM-D5D siRNA nanoparticle on lung cancer cell proliferation, we assessed the expression of proliferation marker Ki67 in A549 cells by immunofluorescence analysis. Ki67 is a widely used marker for evaluating cancer cell proliferation.[22,23] The Ki67-stained immunofluorescence images indicated that the combination of 3WJ-EpCAM-D5D siRNA nanoparticle and DGLA treatment could significantly suppress lung cancer cell proliferation (Figure 2G, $p < 0.05$). This could be attributed to the successful internalization of the 3WJ-EpCAM-D5D siRNA nanoparticle to the lung cancer cells and the subsequent D5D inhibition and 8-HOA production.

However, unlike A549 lung cancer cells, H1299 lung cancer cells have similar protein expression levels of EpCAM but significantly less expression of COX-2 (Figure S4A; $p < 0.001$). Notably, BEAS-2B normal lung epithelial cells have significantly less or no protein expression of EpCAM and COX-2 (Figure S4A). This was further confirmed by the nanoparticle internalization study on both H1299 and BEAS-2B cells under confocal microscopy. Here, only a small fraction of 3WJ-EpCAM-Alexa 647 RNA nanoparticles was observed in BEAS-2B cells compared with the A549 (Figure 2C) and H1299 lung cancer cells (Figure S4C). This phenomenon could be attributed to the relatively lower expression of EpCAM in BEAS-2B cells. In the case of H1299 cells, DGLA and 3WJ-EpCAM-D5D siRNA nanoparticle failed to improve the cell viability and survival fraction, indicating the COX-2-dependent role on eliciting the effectiveness of 3WJ-EpCAM-D5D siRNA nanoparticle (Figures S5A and S5B). The GC-MS analysis revealed that the 3WJ-EpCAM-D5D siRNA nanoparticle did not improve the formation of 8-HOA in BEAS-2B cells (Figure S6A). Additionally, we did not observe the significant effect of the combination of DGLA and 3WJ-EpCAM-D5D siRNA nanoparticle on cell viability, cytotoxicity via lactate dehydrogenase (LDH) release assay, and survival fraction of BEAS-2B cells (Figures S6B–S6D). Therefore, the high expression of EpCAM and COX-2 in lung cancer constructed belt-and-braces security to avoid the toxicity of 3WJ-EpCAM-D5D siRNA nanoparticle to normal lung epithelial cells.

3WJ-EpCAM-D5D siRNA Nanoparticles and DGLA Supplementation Inhibited Lung Tumor Growth *In Vivo*

To assess the *in vivo* distribution and effectiveness of the 3WJ RNA nanoparticle, we synthesized two different nanoparticles as described in the previous study.[15] For the biodistribution test, 3WJ-EpCAM-Alexa 647 nanoparticle was synthesized without the therapeutic module (D5D siRNA), whereas the 3WJ-EpCAM-D5D siRNA nanoparticle was synthesized for assessing the efficacy of the nanoparticle, which harbored targeting module and D5D siRNA. The *in vivo* distribution of 3WJ RNA nanoparticle was determined by tracking the Alexa 647 signal in the nude mice with xenograft lung tumors. The xenograft tumor showed a much higher signal than other organs when 3WJ-EpCAM-Alexa 647 nanoparticles were injected into the

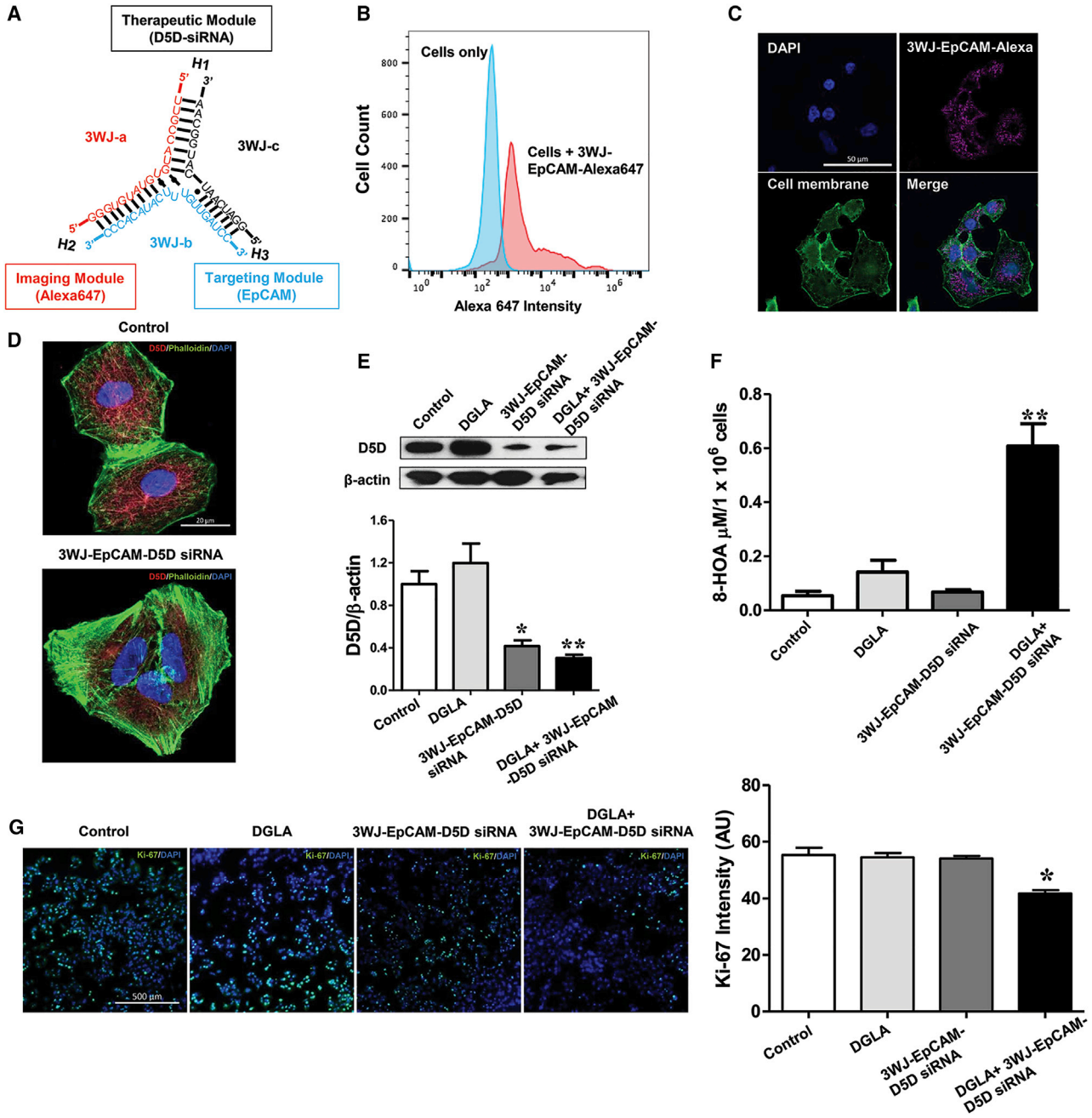

Figure 2. 3WJ-EpCAM-D5D siRNA Nanoparticle Suppressed A549 Lung Cancer Cell Proliferation

(A) Schematic presentation of the 3WJ-RNA nanoparticle structure, which shields three different modules, D5D siRNA (therapeutic module), Alexa 647 (imaging module), and EpCAM aptamer (targeting module). (B) The RNA nanoparticle cell-binding test via flow cytometry was performed on A549 cells. The red peak represents A549 cells treated with 3WJ-EpCAM aptamer-Alexa 647 nanoparticle. A549 cells incubated with PBS (without any treatment) served as control (blue peak). (C) Confocal microscopy in Airyscan 2 modes to visualize the cellular internalization of 3WJ-EpCAM-Alexa 647 nanoparticles within A549 cells. Phalloidin was stained with Alexa 488 (green) and DAPI for cell nuclei. Scale bars, 50 μm. (D) Confocal microscopy images of D5D fluorescence signals in A549 cells treated with 100 nM 3WJ-EpCAM nanoparticles (without the therapeutic module, served as the control) or 3WJ-EpCAM-D5D siRNA nanoparticles (with therapeutic module) for 48 h. Scale bars, 20 μm. (E) Relative protein expression of D5D in A549 cells. The relative expression of D5D to β-actin in the control group was normalized to 1. (F) GC/MS analysis of 8-HOA concentration in A549 cells treated with DGLA (100 μM) and 3WJ-EpCAM-D5D siRNA nanoparticle (100 nM) for 48 h. (G) Immunofluorescence images and quantification of Ki67 relative intensity within A549 cells by confocal microscopy after the treatment of DGLA (100 μM) and 3WJ-EpCAM-D5D siRNA nanoparticle (100 nM) for 48 h. The expression of Ki67 was marked in green, and DAPI for cell nuclei. Scale bars, 500 μm. n = 3 (B and E); n = 6 (C, D, F, and G). Data represent mean ± SEM. $^{**}p < 0.01$, $^{*}p < 0.05$ versus control group.

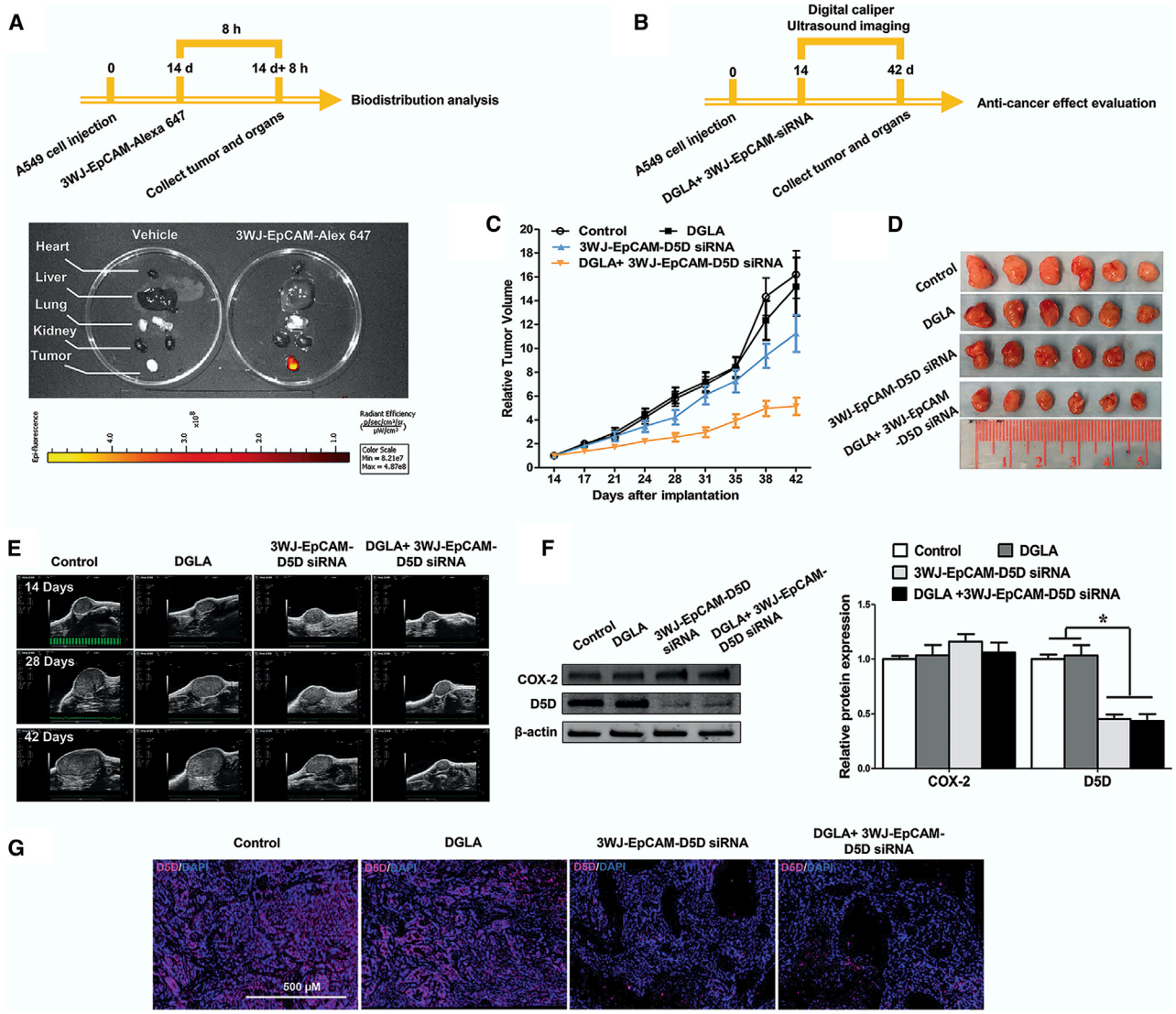

Figure 3. 3WJ-EpCAM-D5D siRNA Nanoparticles and DGLA Combination Suppress A549 Tumor Growth *In Vivo*

(A) Study design and *in vivo* biodistribution assay of 3WJ-EpCAM-Alexa 647 nanoparticles (20 μM for 8 h) in vital organs and xenograft A549 tumor tissues from mice by *In Vivo* Imaging System (IVIS) Spectrum station. The red and yellow indicated a higher signal of 3WJ-EpCAM-Alexa 647 nanoparticles. (B) Study design for evaluating the anti-cancer effect of 3WJ-EpCAM-D5D siRNA nanoparticle. (C) Relative tumor volume of nude mice treated with DGLA (5 mg/mouse, oral gavage, every day) and 3WJ-EpCAM-D5D siRNA nanoparticles (intravenous injection, twice a week, 20 μM in 50 μL PBS) from the start of treatment (14 days) to the end of treatment (42 days). A digital caliper was used to measure the relative tumor volume during the treatment. (D) Images of harvested tumors at the end of 4 weeks of DGLA and 3WJ-EpCAM-D5D siRNA nanoparticle treatment. (E) Ultrasound images of tumor growth in mice during 4-week treatment. Notably, day 14 indicates the first day of the treatment after cancer cell implantation; day 42 is the last day before sacrifice. (F) Relative expression of COX-2 and D5D in tumor tissues after 4 weeks of treatment of DGLA (5 mg/mouse) and 3WJ-EpCAM-D5D siRNA nanoparticles (20 μM). Relative expression of proteins was normalized by β-actin. (G) The D5D relative intensity in tumor tissues after 4 weeks of treatment of DGLA (5 mg/mouse) and 3WJ-EpCAM-D5D siRNA nanoparticles (20 μM) was measured by immunofluorescence analysis. The expression of D5D was marked in violet and DAPI for cell nuclei. Scale bars, 500 μm. n = 3 (A, E, and F); n = 6 (C, D, and G). Data represent mean ± SEM. *p < 0.05 versus control group.

nude mice (Figure 3A). The whole-body fluorescence images revealed the process of how 3WJ-EpCAM-Alexa 647 nanoparticles distributed from the circulatory system to specifically into the tumor. At 1 h post-injection of 3WJ-EpCAM-Alexa 647 nanoparticles, the signal of nanoparticles was observed all over the body of the nude mouse. However, the signal was preserved in the tumors rather than other organs at 4–8 h post-injection (Figure S2A) of 3WJ-EpCAM-Alexa 647 nanoparticles.

To evaluate the effectiveness of 3WJ RNA nanoparticle on tumor reduction, we treated the separate set of the mice with DGLA and/or 3WJ-EpCAM-D5D siRNA nanoparticle for 4 weeks (see

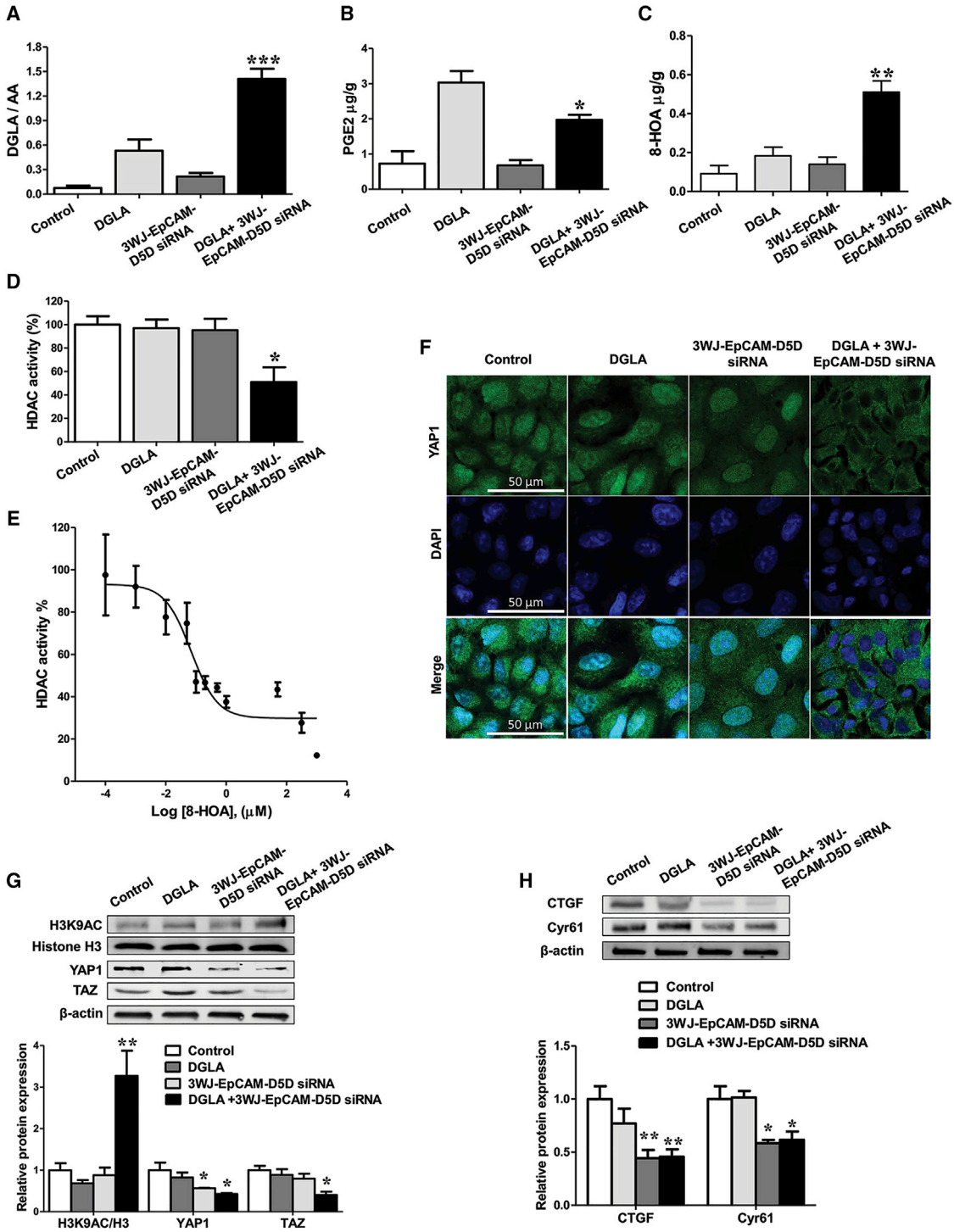

Figure 4. 3WJ-EpCAM-D5D siRNA Nanoparticles and DGLA Combination Promoted 8-HOA Production in A549 Xenograft Tumor Tissues

(A) LC/MS quantification of DGLA versus AA ratio from A549 tumor tissues. The tumor tissues were obtained from mice treated with DGLA (5 mg/mouse, oral gavage, every day) and 3WJ-EpCAM-D5D siRNA nanoparticles (intravenous injection, twice a week, 20 μM in 50 μL PBS) for 4 weeks. (B) Prostaglandin E2 (PGE2, μg/g) concentration in tumor tissues was quantified by LC/MS. (C) GC/MS quantification of 8-HOA from tumor tissues. (D) HDAC activity in A549 xenograft tumors after 4 weeks of treatment. (E) Dose-response curve of HDAC activity to 8-HOA treatment in A549 cells (*in vitro*). (F) Confocal microscopy images of YAP1 fluorescence signals in A549 cells treated with 100 μM DGLA and/or 100 nM 3WJ-EpCAM-D5D siRNA nanoparticles (with therapeutic module) for 48 h. YAP1 is shown in green, and DAPI for nuclei. Scale bars, 50 μm. (G)

(legend continued on next page)

Figure 3B). During the treatment period, tumor size was measured by ultrasound (Figure 3E) and digital caliper (Figure 3C). Compared with the control group, there is about a 61% reduction of tumor volume in the DGLA and 3WJ-EpCAM-D5D siRNA nanoparticle-treated nude mice (Figure 3C). To validate the *in vivo* efficiency of 3WJ-EpCAM-D5D siRNA nanoparticle, we evaluated D5D protein expression in tumor tissues by western and immunofluorescence analyses. Administration of 3WJ-EpCAM-D5D siRNA nanoparticles resulted in a significant decrease in D5D expression in tumors as shown in Figures 3F and 3G ($p < 0.05$), indicating that the D5D siRNA efficiency was preserved by the 3WJ-EpCAM-D5D siRNA nanoparticle in the nude mice with A549 tumors. Additionally, the EpCAM protein expression in tumor tissues was measured by western analysis and suggested that neither DGLA nor 3WJ-EpCAM-D5D siRNA nanoparticle could alter the expression level of EpCAM in tumor tissues (Figure S4B). To monitor the COX-2 status in tumors, we determined the COX-2 protein expression in the xenograft tumors by western analysis. However, neither the 3WJ-EpCAM-D5D siRNA nanoparticle nor DGLA influenced the intensive expression of COX-2, which is critical for catalyzing the 8-HOA production from DGLA peroxidation in tumors (Figure 3F).

3WJ-EpCAM-D5D siRNA Nanoparticles Promoted 8-HOA Formation and Inhibited HDAC Activity

To investigate the mechanism of the 3WJ-EpCAM-D5D siRNA nanoparticle on lung tumors, we analyzed the DGLA, AA, PGE2, and 8-HOA concentrations in tumor tissues by using LC/MS and GC/MS. The high DGLA versus AA ratio indicated that the production of AA from DGLA was obstructed by the treatment of 3WJ-EpCAM-D5D siRNA nanoparticle (Figure 4A; $p < 0.001$). Despite the constant high COX-2 expression in tumors, the production of PGE2 was limited due to low AA concentration. Therefore, compared with the DGLA treatment group, the PGE2 in tumor tissues was decreased in the mice treated with DGLA and 3WJ-EpCAM-D5D siRNA nanoparticles (Figure 4B; $p < 0.05$), whereas the 8-HOA was increased to 0.51 ± 0.06 μg/g in the DGLA and 3WJ-EpCAM-D5D siRNA nanoparticle-treated group (Figure 4C; $p < 0.01$) because of the shifted metabolic pathway. However, the mechanism of 8-HOA on lung cancer is unknown. To decipher the possible mechanisms, we measured the HDAC activity in the tumor tissues using an HDAC activity kit. HDAC activity was significantly suppressed in the tumors treated with DGLA and the 3WJ-EpCAM-D5D siRNA nanoparticle (Figure 4D; $p < 0.05$) without influencing the activity of sirtuin (Figures S7A–S7C), indicating a sirtuin-independent inhibitory mechanism. Moreover, western analysis was used to assess the expression of acetyl-histone H3 (Lys9) (H3K9AC) in the tumor tissues. The significantly higher H3K9AC-to-histone H3 protein expression ratio (H3K9AC/H3) in tumor tissues indicated that the DGLA and 3WJ-EpCAM-D5D siRNA nanoparticle could inhibit the HDAC-catalyzed deacetylation in lung tumors (Figure 4G; $p < 0.01$). This phenomenon of inhibition of HDAC activity has been implicated in modulating transcription and in inducing apoptosis in many cancer progressions.[24,25] To elucidate the mechanism of 8-HOA on HDAC activity, we determined the HDAC activity to the 8-HOA dose-response curve in A549 cells by HDAC activity kit at 48 h of 8-HOA administration. About 44% HDAC activity was suppressed in the A549 cells treated with 0.5 μM 8-HOA (Figure 4E), which is highly consistent with the *in vitro* 8-HOA profile (0.61 ± 0.08 μM) in the A549 cells treated with the 3WJ-EpCAM-D5D siRNA nanoparticle (see Figure 2F). The 3WJ-EpCAM-D5D siRNA nanoparticle increased the 8-HOA concentration in A549 cells to ~0.6 μM, which is an effective dose that could lead to more than half loss of HDAC activity in A549 cells. The strong correlation between the treatment of 3WJ-EpCAM-D5D siRNA nanoparticle and the inhibition of HDAC activity is possibly attributed to the formation of 8-HOA, which shared a partial structure with the aliphatic acid HDAC inhibitors.[26]

In the progression of lung cancer, YAP1/TAZ can be activated and transferred into nuclear to promote cancer cell growth and proliferation.[27–32] To investigate the role of YAP1/TAZ in the treatment, we performed the immunofluorescence analysis to determine the cellular localization of YAP1 in A549 cells. The immunofluorescence images showed that most of the YAP1 was sequestered to the cytoplasm after the treatment of DGLA and nanoparticle, thereby inhibiting the YAP1 nuclear translocation (Figure 4F). Not only did co-treatment of DGLA and 3WJ-EpCAM-D5D siRNA nanoparticle influence YAP1 cellular localization, but this combination also significantly decreased the protein expression of YAP1 and TAZ in the tumor tissues (Figure 4G, $p < 0.05$). Additionally, we also observed that 3WJ-EpCAM-D5D siRNA nanoparticle alone or combined with DGLA could significantly decrease the protein expression of CTGF and Cyr61, which are downstream markers of YAP1/TAZ (Figure 4H, $p < 0.05$). The YAP1/TAZ has been identified as the major downstream effector of the Hippo pathway. The activated Hippo pathway has been reported to prevent YAP1/TAZ nuclear translocation and overexpression.[27,28] Therefore, the suppression of YAP1/TAZ expression and nuclear translocation observed by western and immunofluorescence analyses indicated that the Hippo pathway could be activated by DGLA and 3WJ-EpCAM-D5D siRNA nanoparticle in lung tumor.

Effect of 3WJ-EpCAM-D5D siRNA Nanoparticles on Lung Cancer Apoptosis and Metastasis

The activation of the Hippo pathway has been reported to lead to apoptosis and inhibit cancer cell proliferation.[27,28] For *in vivo* study,

Expression of acetyl-histone H3 (H3K9AC), histone H3, YAP1, and TAZ in A549 tumors after 4-week treatment of DGLA (5 mg/mouse) and 3WJ-EpCAM-D5D siRNA nanoparticles (20 μM). The expression of H3K9AC was normalized with the expression of histone H3 in corresponding groups. The protein expression ratio of H3K9AC to histone H3 was shown as H3K9AC/H3. Relative expression of proteins to β-actin was normalized to 1. (H) Expression of connective tissue growth factor (CTGF) and cysteine-rich protein 61 (Cyr61) in A549 tumors after 4-week treatment of DGLA (5 mg/mouse) and 3WJ-EpCAM-D5D siRNA nanoparticles (20 μM). Relative expression of proteins to β-actin was normalized to 1. n = 3 (A–D and F–H); n = 12 (E). Data represent mean ± SEM. ***$p < 0.001$, **$p < 0.01$, *$p < 0.05$ versus control group.

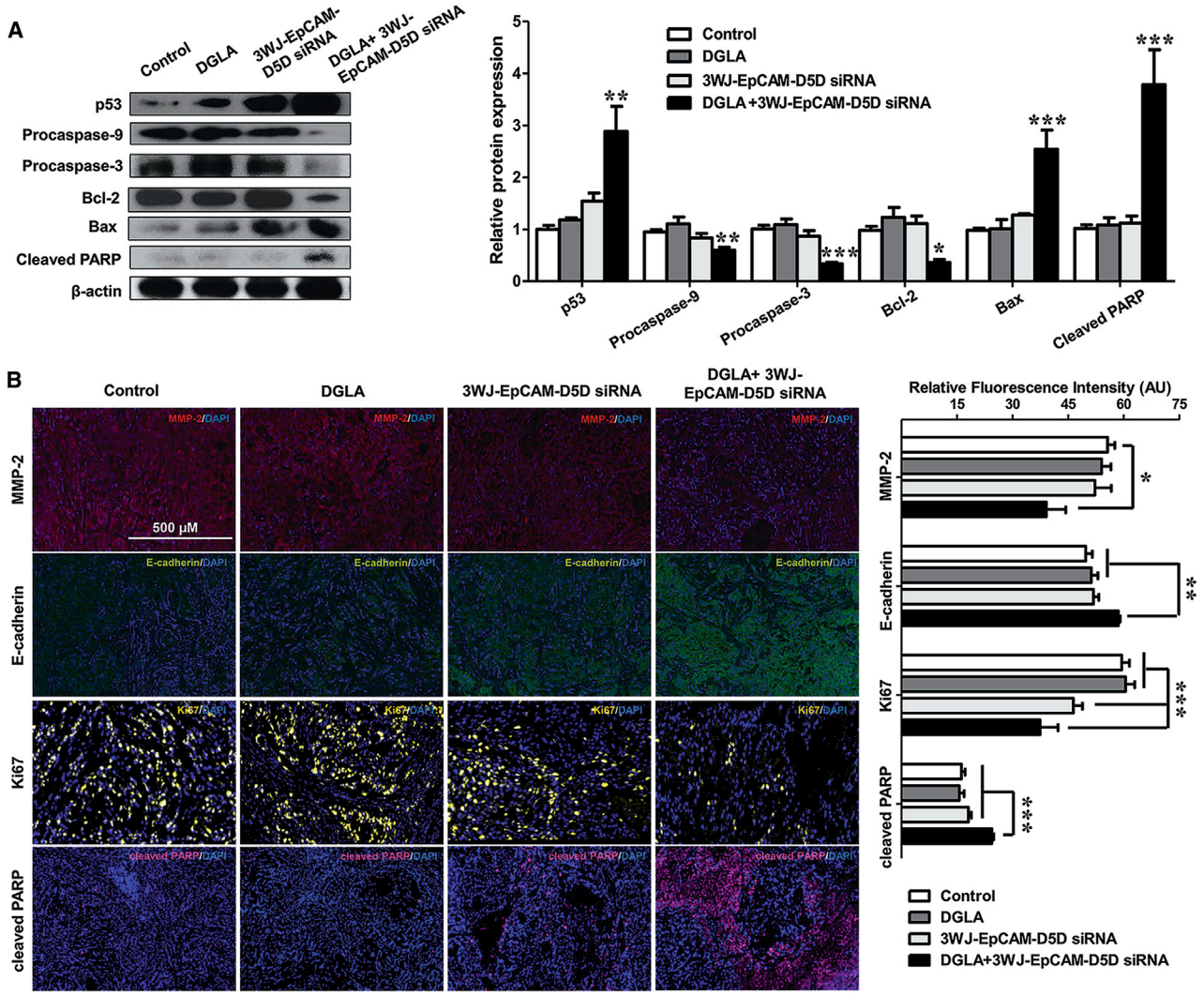

Figure 5. Effect of DGLA Supplementation and 3WJ-EpCAM-D5D siRNA Nanoparticles on A549 Xenograft Tumor Apoptosis, Proliferation, and Metastasis

(A) Expression of p53, procaspase-9, procaspase-3, Bcl-2, Bax, and cleaved PARP expression in A549 tumors treated with DGLA (5 mg/mouse, oral gavage, every day) and 3WJ-EpCAM-D5D siRNA nanoparticles (intravenous injection, twice a week, 20 μM in 50 μL PBS) for 4 weeks. Relative protein expression was normalized with β-actin. (B) Immunofluorescence images and quantification of MMP-2, E-cadherin, Ki-67, and cleaved PARP in tumor tissues after 4 weeks of treatment of DGLA (5 mg/mouse) and 3WJ-EpCAM-D5D siRNA nanoparticles (20 μM). Expression of MMP-2 was shown in red, E-cadherin in green, Ki-67 in yellow, cleaved PARP in violet, and cell nuclei were counter-stained with DAPI. Scale bars, 500 μm. n = 3 (A and B). Data represent mean ± SEM. ***p < 0.001, **p < 0.01, *p < 0.05 versus control group.

apoptosis was assessed by western or immunofluorescence analysis of the proteins like procaspase-9, procaspase-3, poly(ADP-ribose) polymerase (cleaved PARP), Bcl-2, and Bcl-2-associated X protein (Bax) in tumor tissues. The expressions of procaspase-9 and procaspase-3 were significantly decreased in the tumor tissues treated with DGLA and 3WJ-EpCAM-D5D siRNA nanoparticle (Figure 5A, $p < 0.01$), indicating the upregulation of the intrinsic apoptosis pathway. However, the expression of tumor suppressor p53 was significantly increased in the tumor tissues administrated with DGLA and 3WJ-EpCAM-D5D siRNA nanoparticle (Figure 5A, $p < 0.01$). p53 has been reported to regulate the expression of Bax, which is an apoptotic activator.[33] Compared with the control group, the treatment of DGLA and 3WJ-EpCAM-D5D siRNA nanoparticle significantly upregulated the expression of Bax ($p < 0.001$), but suppressed Bcl-2 (anti-apoptotic regulator, $p < 0.05$) in lung tumor tissues (Figure 5A). Additionally, the higher cleaved PARP expression in nanoparticle-treated tumors indicated the combination of DGLA and 3WJ-EpCAM-D5D siRNA nanoparticle could also induce apoptosis in a caspase-independent manner (Figures 5A and 5B, $p < 0.001$). Furthermore, to evaluate cell proliferation, we performed the immunofluorescence analysis on tumor samples by staining with Ki67. The significant lower intensity of Ki67 was found in tumor tissues treated with DGLA and 3WJ-EpCAM-D5D siRNA nanoparticle, suggesting the suppression of cancer proliferation (Figure 5B, $p < 0.001$).

The high mortality of lung cancer is attributed to the high incidence of metastases.[34] Matrix metalloproteinase-2 (MMP-2) has been reported that can break the extracellular matrix (ECM) by degrading type IV collagen. The breakdown of the ECM and basement membrane could permit cancer cells to spread to other tissues and organs.[35–37] To evaluate the MMP-2 expression, we performed the immunofluorescence staining on tumor tissues from nude mice treated with DGLA and 3WJ-EpCAM-D5D siRNA nanoparticle. The immunofluorescence images of tumor tissues indicated that the MMP-2 expression was suppressed by the treatment of DGLA and 3WJ-EpCAM-D5D siRNA nanoparticle (Figure 5B, $p < 0.05$). The lower expression of MMP-2 implicated possible less damage to ECM and diminished metastases in tumor tissues treated with DGLA and 3WJ-EpCAM-D5D siRNA nanoparticle. On the contrary, the dysfunction of epithelial cadherin (E-cadherin) could disrupt cell-cell adhesion that might lead to metastases.[38–41] We observed that the immunofluorescence intensity of E-cadherin was increased in the tumor tissues by administration of DGLA and 3WJ-EpCAM-D5D siRNA nanoparticle (Figure 5B, $p < 0.01$), representing relative higher integrity of adherens junctions and depressed metastases.

The safety assessment was investigated by monitoring the body weight of nude mice during the treatment, measuring the alanine aminotransferase (ALT) and aspartate aminotransferase (AST) activity, and hematoxylin and eosin (H&E) staining on major organs at the end of the treatment. During 4 weeks of the treatment, no significant difference has been found in body weight between the control group and any other nanoparticle treatment group (Figure S2B). Additionally, all of the nanoparticle-treated nude mice have the serum AST and ALT activity within the normal range (normal levels presented in the red line), indicating that either 3WJ-EpCAM-D5D siRNA nanoparticle or nanoparticle combined with DGLA did not have significant hepatotoxicity in 4 weeks of treatment (Figure S2C). The H&E staining of organ sections, collected from nude mice at the end of treatment, suggested that 3WJ-EpCAM-D5D siRNA did not result in any severe morphological damage to major organs (Figure S3). Therefore, the 3WJ-EpCAM-D5D siRNA nanoparticle was safe and effective and held the great promise for the clinical translation of lung cancer therapy.

DISCUSSION

We have previously demonstrated the effect of D5D siRNA knockdown on colon and pancreatic cancers *in vitro*.[6,8] However, siRNA could be attacked by nuclease when administrated *in vivo*. Additionally, the siRNA tends to distribute into the kidney rather than other organs. Therefore, the application of siRNA could be limited by its low bioavailability and efficiency.[21] To improve the *in vivo* efficiency of siRNA, researchers proposed several nanoparticle-based delivery systems, including liposomes, polymer matrix, and RNA nanoparticle, for cancer therapy. Compared with other nanoparticles, RNA nanoparticles are assembled as a chain of nucleotides, which has excellent biocompatibility.[12] In the safety test, we have not found significant pathologic changes in vital organs from mice treated with 3WJ-EpCAM-D5D siRNA nanoparticle for 4 weeks. It is consistent with the previous safety test of RNA nanoparticles, which incorporated with different functional modules.[13] Additionally, the multivalent structure of 3WJ RNA nanoparticle facilitated the conjugation of D5D siRNA, EpCAM aptamer, and Alexa 647, all in one nanoconstruct. This active and targeted 3WJ RNA nanoparticle showed high affinity and penetrability in the treatment of A549 lung cancer cells. Once into the cytoplasm, the formation of 8-HOA was strongly promoted by 3WJ-EpCAM-D5D siRNA nanoparticle.

The bad diet structure is one of the risk factors of lung cancer progression. In a normal diet, the recommended ratio of omega 6 to omega 3 fatty acid is about 4:1 or less. However, this ratio is much higher in the western diet (20:1). High omega 6 fatty acid uptake is usually considered as the potential inducer in cancer.[42] The omega 6 fatty acids (such as DGLA) can be converted to AA and PGE2 by COX-2-catalyzed peroxidation. Then the produced PGE2 could coactivate epidermal growth factor receptor (EGFR) signaling, resulting in migration via upregulating MMP in cancer cells.[43,44] Of note, in this study, we observed a significant downregulation of MMP-2 expression in lung tumors treated with 3WJ-EpCAM-D5D siRNA nanoparticle. This phenomenon could reflect the inhibition of PGE2 production by D5D knockdown in tumors. Additionally, the 3WJ-EpCAM-D5D siRNA nanoparticle also can promote the 8-HOA formation in lung cancer cells. Consistent with our *in vitro* data, we found that the 3WJ-EpCAM-D5D siRNA nanoparticle could lead to apoptosis but suppress proliferation and migration by inducing 8-HOA formation in lung tumor tissues. By redirecting the pattern of COX-2-catalyzed DGLA peroxidation, we established a strategy for lung cancer therapy, which reverses the trend of 8-HOA/PGE2 production in lung tumors.

8-HOA has been found as a free radical byproduct, which appears to work in an autocrine manner to not only suppress pancreatic and colon cancer growth but also inhibit metastasis.[9] Consistent with previous studies, we demonstrated that 8-HOA also could inhibit HDAC activity in A549 lung cancer cells. HDAC plays a key role in cancer proliferation and apoptosis by decreasing tumor suppressor gene transcription and leading to unchecked cell growth and survival.[25] Therefore, the effect of the 3WJ-EpCAM-D5D siRNA nanoparticle on lung cancer proliferation and apoptosis is reasonably attributed to increasing 8-HOA production. Meanwhile, several classic HDAC inhibitors have been reported that could suppress YAP1/TAZ expression in cancer cells.[45] Similarly, 8-HOA, as a potential HDAC inhibitor, also displayed an inhibitory effect on YAP1/TAZ expression and nuclear translocation in A549 cells. It is plausible that the effect of 8-HOA on lung cancer cell proliferation and apoptosis is associated with the activation of the Hippo pathway.

In conclusion, we proposed a therapy regimen for lung cancer that combined the paradigm shift of COX-2 biology with the innovative RNA nanotechnology to deliver the therapeutic D5D siRNA specifically to lung tumors. With EpCAM targeting, the 3WJ RNA nanoparticle conjugated with D5D siRNA could specifically bind and enter the lung cancer cells, resulting in a decrease in D5D expression. By

subverting the DGLA peroxidation, the 8-HOA formed in nanoparticle-treated lung tumors could significantly inhibit the HDAC activity. This potential HDAC inhibitor could further lead to apoptosis and suppress the proliferation and metastasis in lung tumors by inhibiting YAP1/TAZ expression and nuclear translocation. The 3WJ-EpCAM-D5D siRNA nanoparticle strongly suppressed tumor growth and also was devoid of the side effects on other organs. Overall, our strategy generated an effective and safer outcome in lung cancer therapy.

MATERIALS AND METHODS

Cancer Cell Line and Materials

A549, H1299 NSCLC, and BEAS-2 normal lung epithelial cell lines were purchased from the American Type Culture Collection (ATCC, VA, USA). D5D-targeted siRNA, Lipofectamine RNAiMAX transfection reagent, MEM reduced serum medium, and negative control siRNA were bought from Thermo Fisher Scientific (MA, USA). Analytical standard grades of AA-d_8, AA, DGLA, and DGLA-d_6, as well as DGLA ethyl ester (batch number: 0531920-3 used for *in vivo* study), were obtained from Cayman Chemical (MI, USA). SampliQ Silica C18 ODS reverse-phase SPE cartridge was bought from Agilent Technology (CA, USA). Radioimmunoprecipitation assay (RIPA) lysis buffer was purchased from Thermo Fisher Scientific. Fetal bovine serum (FBS) and Dulbecco's modified Eagle's medium (DMEM) were obtained from Hyclone Laboratories (GE Healthcare, IL, USA). For immunofluorescence staining, primary antibodies, Alexa fluor-conjugated secondary antibodies (Alexa 647 and Alexa 488), and Phalloidin-iFluor 488 Reagent were acquired from Abcam (MA, USA). Fluoro-Gel II with DAPI was obtained from Electron Microscopy Sciences (PA, USA). For western analysis, primary antibodies for Bax, p53, Bcl-2, cleaved PARP, procaspase-9, procaspase-3, H3K9AC, and β-actin were bought from Cell Signaling (MA, USA). CTGF, Cyr61, and histone H3 antibodies were purchased from Santa Cruz Biotechnology (TX, USA). IRDye 800 CW Goat anti-Rabbit or anti-Mouse IgG Secondary Antibodies were purchased from LI-COR Biosciences (NE, USA). MTT was obtained from Alfa Aesar (MA, USA). The 3WJ-EpCAM-Alexa 647 nanoparticle was acquired from ExonanoRNA (Columbus, OH, USA). Phosphoramidites and synthesizer reagents for the synthesis of the 3WJ-EpCAM-D5D siRNA nanoparticle were obtained from Glen Research (USA).

siRNA Transfection

D5D siRNA (Silencer Select validated siRNA) transfection was conducted on A549 cells as described in the previous study.[6] In brief, 3×10^5 A549 cells were seeded into each well of a six-well plate for overnight incubation. Then the DMEM cell culture medium was removed, and cells were washed with phosphate-buffered saline (PBS) solution. Transfection mixture containing D5D siRNA (D5D-*KD*, 150 nM in 500 μL) or the same volume of negative control siRNA (*NC-si*, as control) and Lipofectamine RNAiMAX transfection reagent (500 μL) were treated to A549 cells for 6 h in the incubator. After incubation, the reduced serum medium was replaced by DMEM with 10% (v/v) FBS. At 12, 24, and 48 h post-incubation, the transfected cells were collected to verify the knockdown efficiency (D5D protein expression) of D5D siRNA by using western analysis. The appropriate post-transfection time was determined by comparing the D5D expression of A549 cells at different time points. D5D siRNA-transfected A549 cells were then ready for further treatments (DGLA) and experiments (colony formation and transwell assays).

Colony Formation Assay to Evaluate the Cell Survival

The *NC-si* and D5D siRNA-transfected A549 cells were trypsinized and seeded into the new six-well plates at the density of 1,000 cells/well. Then the cells were randomly assigned into four different groups, including *NC-si* group (transfected with negative control siRNA), *NC-si* + DGLA group (transfected with negative control siRNA and treated with 100 μM DGLA), D5D-*KD* group (transfected with D5D siRNA), and D5D-*KD* + DGLA group (transfected with D5D siRNA and treated with 100 μM DGLA). After 48 h of DGLA treatment, cells were then washed with PBS and continuously cultured with fresh DMEM with 10% (v/v) FBS for 10 days to allow the formation of colonies. After 10 days, cells were washed with PBS, fixed in 10% neutral buffered formalin for 15 min, and stained with crystal violet for 30 min. The colonies of A549 cells in each well of six-well plates were counted by ImageJ (NIH, Bethesda, MD, USA). The survival fraction was calculated by the equation: the number of colonies in the treatment group divided by the number of colonies in the *NC-si* group.[46]

Transwell Assay to Determine the Cell Migration

The Costar transwell chamber with the non-coated membrane (6.5-mm insert and 24-well plate 8.0-μm polycarbonate membrane) was purchased from Corning Life Sciences. The *NC-si* and D5D siRNA-transfected A549 cells were trypsinized and seeded into the top chamber at the density of 5×10^4 cells/well with DMEM and 10% (v/v) FBS overnight. The medium was then replaced by the fresh DMEM (FBS-free) in the insert, and DMEM with 10% (v/v) FBS in the lower chamber. The treatments were assigned to four groups, including the *NC-si* group, *NC-si* + DGLA group, D5D-*KD* group, and D5D-*KD* + DGLA group. After 48 h of incubation of DGLA, cells were washed with PBS, fixed in 10% neutral buffered formalin for 15 min, and stained with crystal violet for 30 min as described in the previous study.[47] Cotton bud was used to gently remove the residual cells in the inner side of the insert. The migrated cells on the lower surface of the insert were observed and counted in the inverted microscopy (Lecia Microsystems Model DMi8). The percentage of relative migration rate was calculated by the equation: the number of migrated cells in the treatment group divided by the number of migrated cells in the *NC-si* group.[46]

Synthesis of 3WJ RNA Nanoparticles

The 3WJ-EpCAM-Alexa 647 nanoparticle (with imaging module) was purchased from ExonanoRNA to evaluate cell binding, internalization, and *in vivo* biodistribution. The 3WJ-EpCAM nanoparticle (without the therapeutic module, as control for both *in vivo* and *in vitro* study) and 3WJ-EpCAM-D5D siRNA nanoparticle (with

D5D siRNA, for knocking down D5D) were synthesized as described in the previous study.[15] The 3WJa D5D siRNA sense strand (5′-uuG ccA uGu GuA uGu GGG uuA cAu cAu ccA cuc Acu AAA tt-3′) and antisense strand (5′-UUU AGU GAG UGG AUG AUG UCG-3′) were purchased from TriLink BioTechnologies (San Diego, CA, USA). Assembly of 3WJs was performed by mixing corresponding strands at the equimolar molar concentration in TES buffer (10 mM Tris [pH 7.5], 50 mM NaCl, 1 mM EDTA) and annealing at 85°C for 5 min followed by slow cooling to 4°C over about 50 min. 3WJ nanoparticle formation was confirmed on a 12% native PAGE in TBE running buffer (89 mM Tris, 200 mM boric acid, and 5 mM MgCl2). Gels were stained with ethidium bromide (EtBr) followed by imaging by Typhoon FLA 7000 (GE Healthcare).

MTT Assay to Determine the Cell Viability

The dose of 3WJ-EpCAM-D5D siRNA nanoparticle for the *in vitro* study was optimized by MTT assay. The A549 cells were seeded at 8,000 cells/well (in 100 μL medium) into 96-well plates, and overnight incubation was done. The 3WJ-EpCAM-D5D siRNA nanoparticle (1, 10, 100, or 1,000 nM) was treated to each well with the serum-free DMEM for 6 h. The control group was treated with the same volume of the 3WJ-EpCAM nanoparticle. Then the A549 cells were subjected to 100 μM DGLA for 48 h with fresh complete DMEM (10% [v/v] FBS). After treatment with DGLA, each sample received 10 μL 0.5% (w/v) MTT and was incubated for 4 h. The supernatant of each well was replaced with 100 μL DMSO to dissolve the formed crystal. The optical density (OD) value of each well was determined by using a microplate reader at 570/650 nm. The cell viability of the treatment group was normalized by the OD value in the control group.

Cell Binding of 3WJ RNA Nanoparticle

About 3×10^5 A549 cells were trypsinized and washed with PBS. After centrifugation (3,000 rpm for 5 min), A549 cells were resuspended in the 100 μL PBS solution or 100 nM 3WJ-EpCAM-Alexa 647 nanoparticle (in 100 μL PBS) solution. A549 cells were then incubated at 37°C for 2 h. After incubation, cells were washed and resuspended in PBS, followed by flow cytometry analysis (BD Accuri C6 Flow Cytometer) of Alexa 647 intensity.[15] The population of control A549 cells was represented as a blue peak. The red peak represented the cell population with the treatment of 3WJ-EpCAM-Alexa 647 nanoparticle.

Internalization of 3WJ RNA Nanoparticles within Cells

A549 cells were trypsinized and seeded into each well (300 μL/well) of μ-Slide 8 Well (ibidi) with complete DMEM (10% [v/v] FBS) overnight. 200 nM 3WJ-EpCAM-Alexa 647 nanoparticle (in 100 μL PBS) was treated to A549 cells for 4 h at 37°C. Then the cells were washed with a warm PBS-Calcium solution and fixed with a 4% neutral buffered formalin solution for 30 min. Phalloidin-iFluor 488 Reagent was then added to each well for 30 min to stain the actin filaments of A549 cells. The reagent was then removed and washed with a PBS-calcium solution three times. Fluoro-Gel II with DAPI was applied to each well for the staining of the nucleus. The μ-Slide 8 Well was observed under confocal microscopy (LSM900 with Airyscan 2; Carl Zeiss Microscopy) to track the distribution of 3WJ-EpCAM-Alexa 647 nanoparticles.[15]

In Vivo Targeting of 3WJ RNA Nanoparticles in the Nude Mice

Six-week-old homozygous nude mice (NU/J, Stock No.: 002019) were bought from The Jackson Laboratory (Sacramento, USA). Mice were raised in a pathogen-free Innovive IVC system a week before the study. Before the *in vivo* study, A549 cells were shipped to IDEXX BioResearch for IMPACT rodent pathogen testing as required of the Institutional Animal Care and Use Committees at North Dakota State University. In brief, 2×10^6 pathogen-free A549 (suspended in 100 μL FBS-free DMEM) cells were injected into mouse hind flank subcutaneously by using BD 1 mL TB syringe (25G × 5/8; BD, NJ, USA). The mice were then fed a standard diet (Teklad Global 18% Protein Rodent Diet; ENVIGO) for 2 weeks to allow the xenograft tumor formation. After 2 weeks, 20 μM 3WJ-EpCAM-Alexa 647 nanoparticle (in the 50 μL PBS) or 3WJ-EpCAM nanoparticle (in the same volume, served as a control) was administrated to the nude mice by intravenous (i.v.) injection (0.5 mL U-100 Insulin Syringe, 29G × 1/2; BD, NJ, USA). At 1, 4, and 8 h post-injection, the mice were anesthetized by isoflurane (3% in 100% O_2 for induction, 2% in 100% O_2 for maintenance). The relative fluorescence intensity of nanoparticle in the nude mouse was measured by the NIR imaging system as described in the previous study.[48] After 8 h of the injection of 3WJ-EpCAM-Alexa 647 nanoparticles, the mice were euthanized, and the major organs (heart, liver, lung, spleen, and kidney) and tumors were harvested. The *in vivo* biodistribution of 3WJ-EpCAM-Alexa 647 nanoparticles (in organs and tumors) was determined by the *In Vivo* Imaging System (IVIS) Spectrum station.[13,15]

Mouse Xenograft Tumor Model to Evaluate the Effect of 3WJ RNA Nanoparticle

Six-week-old nude mice (NU/J, Stock No.: 002019) obtained from The Jackson Laboratory were also used to investigate the *in vivo* effect of the 3WJ-EpCAM-D5D siRNA nanoparticle on lung tumors. Mice were raised in a pathogen-free Innovive IVC system a week before the study. All of the animal experiments in this study were approved by the Institutional Animal Care and Use Committees at North Dakota State University. After 2 weeks, the A549 cells (2×10^6, suspended in 100 μL FBS-free DMEM) were injected to the hind flank subcutaneously by using BD 1 mL TB syringe (25G × 5/8; BD, NJ, USA). The nude mice were randomly assigned into different treatment groups, including control group (treated with the 3WJ-EpCAM nanoparticle, i.v. injection, 0.5 mL U-100 Insulin Syringe, 29G × 1/2, twice a week, 20 μM in 50 μL PBS), DGLA group (5 mg/mouse, oral gavage, 20 gauge polypropylene feeding tubes, every day), 3WJ-EpCAM-D5D siRNA nanoparticle group (i.v. injection, 0.5 mL U-100 Insulin Syringe, 29G × 1/2, twice a week, 20 μM in 50 μL PBS), and DGLA+ 3WJ-EpCAM-D5D siRNA nanoparticle group.[49] All of the treatments were for 4 weeks. At the end of the treatment, nude mice were euthanized with an overdose of pentobarbital (200 mg/kg, intraperitoneally [i.p.]). Tumor tissues, vital organs, and blood were collected from mice. The serum was isolated by centrifuged blood

at 2,500 rpm for 15 min. All of the samples were immediately tested or frozen in the −80°C refrigerator for storage.

Tumor Size Measurements

The xenograft tumor size was measured by a digital caliper twice a week since the first day of the nanoparticle treatment (2 weeks back from cancer cell injection) to determine relative tumor volume (L × W^2/2, where L is longest axis and W is the shortest axis). The tumors were also visualized by the Vevo 3100 VisualSonics Imaging System (FUJIFILM VisualSonics, Toronto, ON, Canada) weekly.[49]

Quantification of DGLA, AA, and PGE2 by LC/MS

The concentrations of DGLA, AA, and PGE2 in A549 cells or tumor tissues were determined by LC/MS as described in the previous studies.[6,15,47,50] For the *in vitro* test, 3.0 × 10^5 A549 cells were seeded into each well of six-well plates, followed with D5D siRNA transfection or treatment of nanoparticle. For siRNA transfection, A549 cells were randomly assigned to six groups with different treatments with 100 μM DGLA for 12, 24, and 48 h. For nanoparticle treatment, A549 cells were randomly assigned to four groups with different treatments (for 48 h), including control group (treated with the 3WJ-EpCAM nanoparticle, 100 nM), DGLA group (100 μM), 3WJ-EpCAM-D5D siRNA nanoparticle group (100 nM), and DGLA + 3WJ-EpCAM-D5D siRNA nanoparticle group. At different treatment durations (12, 24, or 48 h for D5D siRNA; 48 h for nanoparticle), A549 cells were scratched off from the plate and collected with 1 mL cell culture medium. The medium and debris were then blended with 0.45 mL LC-MS grade methanol and 1.55 mL water to make a 15% methanol solution (total 3 mL). After mixing with the internal standards (5.0 μL DGLA-d_6, AA-d_8, and PGE2-d_9 for each sample), the mixture was purified by using the solid-phase extraction (SPE; SampliQ Silica C18 ODS). The analysis system consisting of the high-performance liquid chromatography (HPLC) system (Agilent 1200 series) and LC/MSD SL ion trap mass (Agilent 6300) was used to determine DGLA, AA, and PGE2 concentration in the collected samples (in ethanol). The internal standard curve was determined by analyzing mixtures consisting of DGLA, AA, and PGE2 at different concentrations, and DGLA-d_6, AA-d_8, and PGE2-d_9 (constant concentration). The concentration of DGLA, AA, and PGE2 in cell samples was determined by the standard curve (comparing the peak areas with their internal standards). For *in vivo* study, the tumor tissues were crushed in mortar after being frozen in the liquid nitrogen. Then 1 mL tissue lysis was prepared for LC/MS as the same procedures as the quantification *in vitro*.

Quantification of 8-HOA via GC/MS

For *in vitro* study, 3.0 × 10^5 A549 cells were seeded into six-well plates, followed with siRNA transfection or administration of 100 nM 3WJ-EpCAM-D5D siRNA nanoparticle with 100 μM DGLA. For siRNA transfection, A549 cells were randomly assigned to different treatments with 100 μM DGLA for 12, 24, and 48 h. For nanoparticle treatment, A549 cells were randomly assigned to four groups with different treatments (for 48 h), including control group (treated with the 3WJ-EpCAM nanoparticle, 100 nM), DGLA group (100 μM), 3WJ-EpCAM-D5D siRNA nanoparticle group (100 nM), and DGLA + 3WJ-EpCAM-D5D siRNA nanoparticle group. At the end of treatment, cells and 1 mL medium were collected and mixed with methanol (500 μL), hexanoic acid (1 μM, internal standard), hydrochloric acid (1.0 N), and dichloromethane (3 mL). The organic layer was collected and combined with the organic layer from another repeated extraction. The dichloromethane was removed by a vacufuge concentrator. The residual was reconstituted in 1.0% diisopropylethylamine (50 μL), reacted with 1.0% pentafluorobenzyl -bromide in acetonitrile (50 μL) for 30 min, and evaporated to dryness in a vacufuge concentrator. The residual was reconstituted in dichloromethane (100 μL) and analyzed by GC-MS as described in the previous studies.[6,15,47,50] The contents of 8-HOA were determined by using the internal standard curve of hexanoic acid (comparing the peak area with the internal standard). For *in vivo* study, the collected tumor tissues were crushed in a mortar after freezing in the liquid nitrogen. The procedure of 8-HOA quantification is the same as *in vitro*.

Determination of HDAC Activity

The dose-response curve of HDAC activity to 8-HOA was determined *in vitro*. About 3.0 × 10^5 A549 cells were seeded into six-well plates and followed the treatment of 8-HOA in various concentrations (0.0001, 0.001, 0.01, 0.05, 0.1, 0.2, 0.5, 1, 50, 315, and 1,000 μM) for 48 h. Then the cell lysate was prepared in RIPA lysis buffer and subjected to HDAC activity colorimetric assay kit (catalog #K331-100; BioVision) as the given protocol. Tumor tissue homogenate was prepared to assess the HDAC activity by using the same HDAC activity colorimetric assay kit and protocol. Tumors are collected from the following groups: control group (3WJ-EpCAM nanoparticle, 20 μM), DGLA group (5 mg/mouse), 3WJ-EpCAM-D5D siRNA nanoparticle group (20 μM), and DGLA+ 3WJ-EpCAM-D5D siRNA nanoparticle group.

Western Analysis

About 3.0 × 10^5 A549 cells were seeded into six-well plates, followed with D5D siRNA transfection (12, 24, or 48 h) or treatment of 100 μM DGLA and/or 100 nM 3WJ-EpCAM-D5D siRNA nanoparticle for 48 h. Protein was collected by scratching off the cells from plates with RIPA buffer (mixed with protease and phosphatase inhibitor cocktail) on the ice. The supernatant was collected from cell lysates by centrifugation at 12,000 rpm for 10 min. The protein concentration of each sample solution was determined by using Pierce BCA Protein Assay Kit (Catalog No. [Cat #]]: 23250; Thermo Fisher Scientific) as the instruction. The normalized protein samples were mixed with 4× Laemmli Sample Buffer (Cat #161-0747; Bio-Rad Laboratories) and denatured at 95°C for 5 min. Then each sample (containing 80 μg protein) was loaded onto a well of 4%–15% Mini-PROTEAN TGX Stain-Free Gels (Cat #4568084; Bio-Rad Laboratories) for electrophoresis at a constant voltage of 80 V. 0.2 μm polyvinylidene fluoride (PVDF) Transfer Membrane (REF88520; Thermo Fisher Scientific) was immersed in 100% ethanol for 5 min, then transferred to a gel tray containing 30 mL transfer buffer (Trans-Blot Turbo, Cat #10026938; Bio-Rad Laboratories) to equilibrium. The proteins

transferred to the PVDF membrane in the Trans-Blot Turbo Transfer System (Bio-Rad Laboratories) in a 30-min standard program as the instruction manual. After transfer, the membrane was incubated in the 5% non-fat dry milk (sc-2324; Santa Cruz Biotechnology) for 1 h to block the non-specific binding. Then the PVDF membrane was incubated with primary antibody (D5D or β-actin) overnight at 4°C. After washing with 3× of 0.1% Tris-buffered saline with Tween, the membrane was then incubated with the corresponding IRDye secondary antibody. Protein signals were captured by a Li-Cor Odyssey XL System, and densitometry analysis was performed by using ImageJ or Image Studio v.5.2 software. The protein expression in tumor tissues was also determined by western analysis. For *in vivo* study, the collected tumor tissues (100 mg) were frozen in liquid nitrogen and crushed to fine powders by mortar. Then the protein was extracted using RIPA lysis buffer and followed the same procedures as *in vitro*. The western analysis was performed for various proteins, including COX-2, D5D, H3K9AC, histone H3, CTGF, Cyr61, YAP1, TAZ, p53, procaspase-9, procaspase-3, Bcl-2, Bax, and cleaved PARP in the tumor.

Immunofluorescence Analysis

About 5.0×10^4 A549 cells were trypsinized and seeded into each well (300 μL/well) of μ-Slide 8 Well (ibidi) with the complete DMEM (10% (v/v) FBS) overnight. After treatment, A549 cells were fixed by using 4% paraformaldehyde in PBS (pH 7.4) for 20 min. The permeabilization was conducted on μ-Slide by incubating samples for 20 min with PBS containing 0.15% Triton X-100. Cells were incubated with 5% BSA for 1 h to block unspecific binding of antibodies. Followed by blocking, the A549 cells were incubated overnight with primary antibodies at 4°C and then secondary antibodies for 1 h. Phalloidin-iFluor 488 Reagent was used to stain actin filaments. Cell nuclear was stained by DAPI. The fluorescence images of A549 cells were captured by LSM900 confocal microscopy with Airyscan 2 (Carl Zeiss Microscopy). For *in vivo* samples, collected tumor tissues were sent to Advanced Imaging & Microscopy Laboratory in North Dakota State University (NDSU) to cut into slices for fluorescence analysis as described in the previous study.[50] The tumor tissue images were captured with a Zeiss Axio Imager M2 microscope (20×/0.75). The relative intensity of D5D, MMP2, and E-cadherin in tumors was determined by using Image-Pro software (Media Cybernetics). The positive rates of Ki67 and cleaved PARP were illustrated as the Ki67 (or cleaved PARP-positive cells) percentages versus the total number of counted cells.[15]

Statistics

Statistical analysis was conducted using Prism 5 (GraphPad Software, USA). *In vitro* and *in vivo* measurement data were presented as the means ± standard error of the mean (SEM). Multiple comparisons among groups were evaluated using a one-way ANOVA test in Tukey's method. Differences with the minimum of $p < 0.05$ were indicated as statistically significant.

SUPPLEMENTAL INFORMATION

Supplemental Information can be found online at https://doi.org/10.1016/j.omtn.2020.08.024.

AUTHOR CONTRIBUTIONS

Conception and design: S.Y.Q., L.P., and H.S.; Development of methodology: L.P. and H.S.; Acquisition of data: L.P., H.S., and H.W.; Analysis and interpretation of data: L.P., H.S., and H.W.; Writing, review and/or revision of the manuscript: L.P., H.S., H.W., D.S., and V.S.; Technical or material support: H.W., D.S., and V.S.; Study supervision: S.Y.Q. and V.S.

CONFLICTS OF INTEREST

The authors declare no competing interests.

ACKNOWLEDGMENTS

This work was supported by the National Institutes of Health (grant 1R15CA195499-01A1 to S.Y.Q.). We also would like to thank the confocal microscopy core facility under the Dakota Cancer Collaborative on Translational Activity (grant U54GM128729). This work is dedicated to the memory of our wonderful colleague, Dr. Steven Y. Qian, who recently passed away. The authors gratefully acknowledge Dr. Peixuan Guo and Congcong Xu from The Ohio State University (Columbus, OH, USA) for editing the manuscript.

REFERENCES

1. Howlader, N., Noone, A.M., Krapcho, M., Miller, D., Brest, A., Yu, M., Ruhl, J., Tatalovich, Z., Mariotto, A., Lewis, D.R., et al. (2019). SEER Cancer Statistics Review (CSR), 1975–2016 (National Cancer Institute).

2. Gulyas, M., Mattsson, J.S.M., Lindgren, A., Ek, L., Lamberg Lundström, K., Behndig, A., Holmberg, E., Micke, P., and Bergman, B.; Swedish Lung Cancer Study Group (2018). COX-2 expression and effects of celecoxib in addition to standard chemotherapy in advanced non-small cell lung cancer. Acta Oncol. *57*, 244–250.

3. Xin, C., Chu, L., Zhang, L., Geng, D., Wang, Y., Sun, D., Sui, P., Zhao, X., Gong, Z., Sui, M., and Zhang, W. (2019). Expression of Cytosolic Phospholipase A2 (cPLA2)-Arachidonic Acid (AA)-Cyclooxygenase-2 (COX-2) Pathway Factors in Lung Cancer Patients and Its Implication in Lung Cancer Early Detection and Prognosis. Med. Sci. Monit. *25*, 5543–5551.

4. Groen, H.J., Sietsma, H., Vincent, A., Hochstenbag, M.M., van Putten, J.W., van den Berg, A., Dalesio, O., Biesma, B., Smit, H.J., Termeer, A., et al. (2009). Randomized, placebo-controlled phase III study of docetaxel plus carboplatin with celecoxib and cyclooxygenase-2 expression as a biomarker for patients with advanced non-small-cell lung cancer: the NVALT-4 study. J. Clin. Oncol *29*, 4320–4326.

5. Solomon, S.D., McMurray, J.J., Pfeffer, M.A., Wittes, J., Fowler, R., Finn, P., Anderson, W.F., Zauber, A., Hawk, E., and Bertagnolli, M.; Adenoma Prevention with Celecoxib (APC) Study Investigators (2005). Cardiovascular risk associated with celecoxib in a clinical trial for colorectal adenoma prevention. N. Engl. J. Med. *352*, 1071–1080.

6. Xu, Y., Yang, X., Zhao, P., Yang, Z., Yan, C., Guo, B., and Qian, S.Y. (2016). Knockdown of delta-5-desaturase promotes the anti-cancer activity of dihomo-γ-linolenic acid and enhances the efficacy of chemotherapy in colon cancer cells expressing COX-2. Free Radic. Biol. Med. *96*, 67–77.

7. Yang, X., Xu, Y., Miskimins, K.W., and Qian, S.Y. (2016). Knocking Down Delta-5 Desaturase and Exploiting High Expression Level of COX-2 to Inhibit Cancer Migration and Invasion. Free Radic. Biol. Med. *100* (*Suppl*), S133.

8. Yang, X., Xu, Y., Brooks, A., Guo, B., Miskimins, K.W., and Qian, S.Y. (2016). Knockdown delta-5-desaturase promotes the formation of a novel free radical by-product from COX-catalyzed ω-6 peroxidation to induce apoptosis and sensitize pancreatic cancer cells to chemotherapy drugs. Free Radic. Biol. Med. *97*, 342–350.

9. Xu, Y., Qi, J., Yang, X., Wu, E., and Qian, S.Y. (2014). Free radical derivatives formed from cyclooxygenase-catalyzed dihomo-γ-linolenic acid peroxidation can attenuate colon cancer cell growth and enhance 5-fluorouracil's cytotoxicity. Redox Biol. *2*, 610–618.

10. Chen, S.-H., and Zhaori, G. (2011). Potential clinical applications of siRNA technique: benefits and limitations. Eur. J. Clin. Invest. *41*, 221–232.

11. Puri, A., Loomis, K., Smith, B., Lee, J.-H., Yavlovich, A., Heldman, E., and Blumenthal, R. (2009). Lipid-based nanoparticles as pharmaceutical drug carriers: from concepts to clinic. Crit. Rev. Ther. Drug Carrier Syst. *26*, 523–580.

12. Shu, Y., Pi, F., Sharma, A., Rajabi, M., Haque, F., Shu, D., Leggas, M., Evers, B.M., and Guo, P. (2014). Stable RNA nanoparticles as potential new generation drugs for cancer therapy. Adv. Drug Deliv. Rev. *66*, 74–89.

13. Yin, H., Xiong, G., Guo, S., Xu, C., Xu, R., Guo, P., and Shu, D. (2019). Delivery of Anti-miRNA for Triple-Negative Breast Cancer Therapy Using RNA Nanoparticles Targeting Stem Cell Marker CD133. Mol. Ther. *27*, 1252–1261.

14. Lee, T.J., Yoo, J.Y., Shu, D., Li, H., Zhang, J., Yu, J.-G., Jaime-Ramirez, A.C., Acunzo, M., Romano, G., Cui, R., et al. (2017). RNA Nanoparticle-Based Targeted Therapy for Glioblastoma through Inhibition of Oncogenic miR-21. Mol. Ther. *25*, 1544–1555.

15. Xu, Y., Pang, L., Wang, H., Xu, C., Shah, H., Guo, P., Shu, D., and Qian, S.Y. (2019). Specific delivery of delta-5-desaturase siRNA via RNA nanoparticles supplemented with dihomo-γ-linolenic acid for colon cancer suppression. Redox Biol. *21*, 101085.

16. Guo, P., Coban, O., Snead, N.M., Trebley, J., Hoeprich, S., Guo, S., and Shu, Y. (2010). Engineering RNA for targeted siRNA delivery and medical application. Adv. Drug Deliv. Rev. *62*, 650–666.

17. Xu, C., Haque, F., Jasinski, D.L., Binzel, D.W., Shu, D., and Guo, P. (2018). Favorable biodistribution, specific targeting and conditional endosomal escape of RNA nanoparticles in cancer therapy. Cancer Lett. *414*, 57–70.

18. Haque, F., Pi, F., Zhao, Z., Gu, S., Hu, H., Yu, H., and Guo, P. (2018). RNA versatility, flexibility, and thermostability for practice in RNA nanotechnology and biomedical applications. Wiley Interdiscip. Rev. RNA *9*, e1452.

19. Spizzo, G., Fong, D., Wurm, M., Ensinger, C., Obrist, P., Hofer, C., Mazzoleni, G., Gastl, G., and Went, P. (2011). EpCAM expression in primary tumour tissues and metastases: an immunohistochemical analysis. J. Clin. Pathol. *64*, 415–420.

20. Zárate, R., El Jaber-Vazdekis, N., Tejera, N., Pérez, J.A., and Rodríguez, C. (2017). Significance of long chain polyunsaturated fatty acids in human health. Clin. Transl. Med. *6*, 25.

21. Gao, K., and Huang, L. (2013). Achieving efficient RNAi therapy: progress and challenges. Acta Pharm. Sin. B *3*, 213–225.

22. Menon, S.S., Guruvayoorappan, C., Sakthivel, K.M., and Rasmi, R.R. (2019). Ki-67 protein as a tumour proliferation marker. Clin. Chim. Acta *491*, 39–45.

23. Xu, J., Liu, P., Da, J., Hao, J., Peng, W., and Sun, G. (2019). Prognostic value of Ki-67 in stage I non-small-cell lung cancer: A meta-analysis involving 1931 patients. Pathol. Res. Pract. *215*, 855–860.

24. Barneda-Zahonero, B., and Parra, M. (2012). Histone deacetylases and cancer. Mol. Oncol. *6*, 579–589.

25. Ropero, S., and Esteller, M. (2007). The role of histone deacetylases (HDACs) in human cancer. Mol. Oncol. *1*, 19–25.

26. Huang, M., Zhang, J., Yan, C., Li, X., Zhang, J., and Ling, R. (2019). Small molecule HDAC inhibitors: Promising agents for breast cancer treatment. Bioorg. Chem. *91*, 103184.

27. Calses, P.C., Crawford, J.J., Lill, J.R., and Dey, A. (2019). Hippo Pathway in Cancer: Aberrant Regulation and Therapeutic Opportunities. Trends Cancer *5*, 297–307.

28. Hong, W., and Guan, K.-L. (2012). The YAP and TAZ transcription co-activators: key downstream effectors of the mammalian Hippo pathway. Semin. Cell Dev. Biol. *23*, 785–793.

29. Maugeri-Saccà, M., and De Maria, R. (2018). The Hippo pathway in normal development and cancer. Pharmacol. Ther. *186*, 60–72.

30. Plouffe, S.W., Hong, A.W., and Guan, K.-L. (2015). Disease implications of the Hippo/YAP pathway. Trends Mol. Med. *21*, 212–222.

31. Ye, S., and Eisinger-Mathason, T.S.K. (2016). Targeting the Hippo pathway: Clinical implications and therapeutics. Pharmacol. Res. *103*, 270–278.

32. Yu, F.-X., Zhao, B., and Guan, K.-L. (2015). Hippo Pathway in Organ Size Control, Tissue Homeostasis, and Cancer. Cell *163*, 811–828.

33. Marchenko, N.D., Zaika, A., and Moll, U.M. (2000). Death signal-induced localization of p53 protein to mitochondria. A potential role in apoptotic signaling. J. Biol. Chem. *275*, 16202–16212.

34. Mehlen, P., and Puisieux, A. (2006). Metastasis: a question of life or death. Nat. Rev. Cancer *6*, 449–458.

35. Ohbayashi, H. (2002). Matrix metalloproteinases in lung diseases. Curr. Protein Pept. Sci. *3*, 409–421.

36. Qian, Q., Wang, Q., Zhan, P., Peng, L., Wei, S.-Z., Shi, Y., and Song, Y. (2010). The role of matrix metalloproteinase 2 on the survival of patients with non-small cell lung cancer: a systematic review with meta-analysis. Cancer Invest. *28*, 661–669.

37. Osman, N.M., and Osman, W.M. (2016). SDF-1 and MMP2 cross talk in cancer cells and tumor microenvironment in non-small cell lung cancer. Egypt. J. Chest Dis. Tuberc. *65*, 517–525.

38. Paredes, J., Figueiredo, J., Albergaria, A., Oliveira, P., Carvalho, J., Ribeiro, A.S., Caldeira, J., Costa, A.M., Simões-Correia, J., Oliveira, M.J., et al. (2012). Epithelial E- and P-cadherins: role and clinical significance in cancer. Biochim. Biophys. Acta *1826*, 297–311.

39. Taylor, M.D., Liu, Y., Nagji, A.S., Theodosakis, N., and Jones, D.R. (2010). Combined proteasome and histone deacetylase inhibition attenuates epithelial-mesenchymal transition through E-cadherin in esophageal cancer cells. J. Thorac. Cardiovasc. Surg. *139*, 1224–1232, 1232.e1.

40. Rodriguez, F.J., Lewis-Tuffin, L.J., and Anastasiadis, P.Z. (2012). E-cadherin's dark side: Possible role in tumor progression. Biochim. Biophys. Acta *1826*, 23–31.

41. Wong, S.H.M., Fang, C.M., Chuah, L.-H., Leong, C.O., and Ngai, S.C. (2018). E-cadherin: Its dysregulation in carcinogenesis and clinical implications. Crit. Rev. Oncol. Hematol. *121*, 11–22.

42. Huerta-Yépez, S., Tirado-Rodriguez, A.B., and Hankinson, O. (2016). Role of diets rich in omega-3 and omega-6 in the development of cancer. Bol. Méd. Hosp. Infant. México *73*, 446–456.

43. Subbaramaiah, K., and Dannenberg, A.J. (2003). Cyclooxygenase 2: a molecular target for cancer prevention and treatment. Trends Pharmacol. Sci. *24*, 96–102.

44. Pai, R., Soreghan, B., Szabo, I.L., Pavelka, M., Baatar, D., and Tarnawski, A.S. (2002). Prostaglandin E2 transactivates EGF receptor: a novel mechanism for promoting colon cancer growth and gastrointestinal hypertrophy. Nat. Med. *8*, 289–293.

45. Han, H., Yang, B., Nakaoka, H.J., Yang, J., Zhao, Y., Le Nguyen, K., Bishara, A.T., Mandalia, T.K., and Wang, W. (2018). Hippo signaling dysfunction induces cancer cell addiction to YAP. Oncogene *37*, 6414–6424.

46. Xu, Y., Yang, X., Wang, T., Yang, L., He, Y.-Y., Miskimins, K., and Qian, S.Y. (2018). Knockdown delta-5-desaturase in breast cancer cells that overexpress COX-2 results in inhibition of growth, migration and invasion via a dihomo-γ-linolenic acid peroxidation dependent mechanism. BMC Cancer *18*, 330.

47. Yang, X., Xu, Y., Wang, T., Shu, D., Guo, P., Miskimins, K., and Qian, S.Y. (2017). Inhibition of cancer migration and invasion by knocking down delta-5-desaturase in COX-2 overexpressed cancer cells. Redox Biol. *11*, 653–662.

48. Dos Santos Rodrigues, B., Arora, S., Kanekiyo, T., and Singh, J. (2020). Efficient neuronal targeting and transfection using RVG and transferrin-conjugated liposomes. Brain Res. *1734*, 146738.

49. Xu, Y., Yang, X., Gao, D., Yang, L., Miskimins, K., and Qian, S.Y. (2018). Dihomo-γ-linolenic acid inhibits xenograft tumor growth in mice bearing shRNA-transfected HCA-7 cells targeting delta-5-desaturase. BMC Cancer *18*, 1268.

50. Yang, X., Xu, Y., Gao, D., Yang, L., and Qian, S.Y. (2019). Dihomo-γ-linolenic acid inhibits growth of xenograft tumors in mice bearing human pancreatic cancer cells (BxPC-3) transfected with delta-5-desaturase shRNA. Redox Biol. *20*, 236–246.